Realizing Near-Infrared Laser Dyes through a Shift in Excited-State Absorption

Reiko Aoki, Ryutaro Komatsu, Kenichi Goushi, Masashi Mamada, Soo Young Ko, Jeong Weon Wu, Virginie Placide, Anthony d'Aléo, Chihaya Adachi

Realizing Near-Infrared Laser Dyes through a Shift in Excited-State Absorption

Reiko Aoki, Ryutaro KOMATSU, Kenichi Goushi, Masashi MAMADA, Soo Young Ko, Jeong Weon Wu, Virginie Placide, Anthony D'Aléo,* and Chihaya Adachi**

The development of near-infrared (NIR) light sources has attracted much interest due to their attractive applications, such as biosensing and light detection and ranging (LiDAR). In particular, organic semiconductor laser diodes with NIR emission are emerging as a next generation technology. However, organic NIR emitters have generally suffered from a low quantum yield, which has resulted in only a few examples of organic solid-state NIR lasers. In this study, the authors demonstrate a highly efficient NIR emitter based on a boron difluoride curcuminoid structure, which shows a high photoluminescence (PL) quantum yield (Φ_{PL}) at >700 nm and a high fluorescence radiative rate constant in a solid-state film. Amplified spontaneous emission and lasing occurs at >800 nm with very low thresholds. The large redshift of the stimulated emission is attributed to the transition from the lowest excited state to the different vibrational levels of the ground state owing to the overlap between the emission and the singlet–singlet excited-state absorption.

In recent years, organic semiconductor laser diodes (OSLDs) have been intensively researched in terms of materials devel- opment, mechanism investigation, and device optimization.[1–11] OSLDs benefit from advantages such as wavelength tun- ability, mechanical flexibility, and simple fabrication processes compared with conventional inorganic semiconductor lasers, and therefore show great promise in future optoelectronics. Although the first demonstration of a blue OSLD under current excitation was reported based on a blue laser material known as 4,4′-bis([*N*-carbazole]styryl)biphenyl,[12] the development of OSLDs that cover the full color range is highly demanded to expand the possibilities of their applications. In particular, the OSLDs with near-infrared (NIR) emission from 700 to 900 nm are expected to be useful for biosensing and healthcare applications through utilization of the first biological window.[13] The longer wavelengths are also advantageous in fabricating distributed feedback (DFB) resonator structures for lasers because the higher grating periods make the microfabrication processes much easier.[14]

The development of laser dyes that emit light in the NIR region is crucial for the realization of NIR-OSLDs. Thus, it is necessary to have excellent NIR laser dyes that exhibit low thresholds of amplified spontaneous emission (ASE) (E_{th}^{ASE}) and lasing (E_{th}^{Laser}), which are derived from a high fluorescence radiative rate constant (k_r), that is, a high photoluminescence (PL) quantum yield (Φ_{PL}) and short fluorescence lifetime (τ_f). Nevertheless, the Φ_{PL} of NIR emitters are generally very low because of the increase of nonradiative transitions described by the well-established energy gap law.[15,16] Therefore, organic materials showing laser emission in the NIR region are quite limited, especially with regard to low thresholds. Therefore, the development of materials as well as device architectures has remained a challenge.[17] Another issue is a deeper photophysical understanding of the loss mechanisms

R. Aoki, Dr. R. Komatsu, Dr. K. Goushi, Dr. M. Mamada, Prof. C. Adachi
Center for Organic Photonics and Electronics Research (OPERA)
Kyushu University
Fukuoka 819-0395, Japan
E-mail: mamada@opera.kyushu-u.ac.jp; adachi@cstf.kyushu-u.ac.jp
R. Aoki, Dr. R. Komatsu, Dr. K. Goushi, Dr. M. Mamada, Prof. C. Adachi
JST ERATO
Adachi Molecular Exciton Engineering Project c/o Center for Organic Photonics and Electronics Research (OPERA)
Kyushu University
Nishi, Fukuoka 819-0395, Japan
Dr. R. Komatsu
KOALA Tech. Inc.
3-5-12 Fukuoka Industry-Academia Symphonicity (FiaS)
Fukuoka 819-0388, Japan
The ORCID identification number(s) for the author(s) of this article can be found under https://doi.org/10.1002/adom.202001947.
Prof. S. Y. Ko
Department of Chemistry
Ewha Womans University
Seoul 03760, Korea
Prof. J. W. Wu, Dr. V. Placide
Department of Physics
Ewha Womans University
Seoul 03760, Korea
Dr. A. D'Aléo
Building Blocks for Future Electronics Laboratory, UMI 2002
CNRS–Sorbonne Université–Yonsei University
Yonsei University
50 Yonsei-ro, Seodaemun-gu, Seoul 03722, South Korea
E-mail: anthony.daleo@adachilab.com
Prof. C. Adachi
International Institute for Carbon Neutral Energy Research (WPI-I2CNER)
Kyushu University
Nishi, Fukuoka 819-0395, Japan

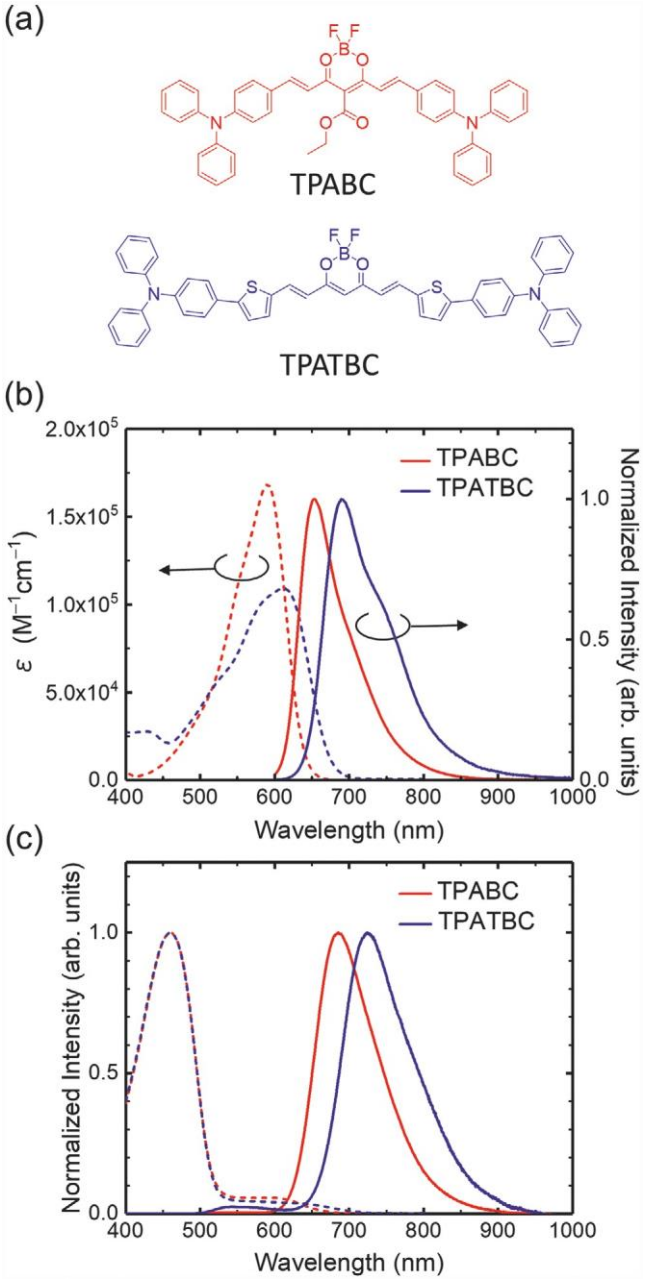

Figure 1. a) Chemical structures of TPABC and TPATBC. UV–vis absorption (dashed lines) and PL (solid lines) spectra for TPABC and TPATBC in b) toluene (1.0×10^{-5} M) and c) the blend films.

based on the intrinsic properties of the materials. In particular, the excited-state absorption that induces exciton quenching is known to be of considerable importance for lasers. However, excited-state absorption has been infrequently investigated for new materials, which has prevented detailed discussions on the relationship between the molecular structures and lasing properties.

So far, one of the best NIR organic laser materials is TPABC (**Figure 1**), which shows a low E_{th}^{ASE} of 7 μJ cm^{-2} at >700 nm. Note that TPABC has been reported to show an excellent organic light-emitting diode (OLED) performance based on the thermally activated delayed fluorescence (TADF) properties.[18] TPABC has a charge transfer (CT) character based on the donor–acceptor interactions between the triphenylamine (TPA) rings and a boron difluoride curcuminoid (BC), which results in emission at longer wavelengths. Although the compounds having a strong CT nature tend to show a broad emission and relatively long τ_f because of large structural relaxations in their excited states, TPABC shows a high Φ_{PL} of >50% and high k_r of $>10^8$ s^{-1} in a host/guest system because the very small bond length alternation in the core structure leads to small relaxation energies.[18] However, a further redshift of emission wavelength to the NIR region is still needed for practical use in some appli- cations, such as photo-thermal therapy at 808 nm and light detection and ranging (LiDAR) sensors at 905 nm.[19–21] The great potential of the BC core in NIR emitters suggests that the synthesis of such compounds for applications should be made possible through an appropriate molecular design.

In this study, we have developed a new NIR laser material, TPATBC, as shown in Figure 1. The introduction of thiophene rings enhances the donor–acceptor interaction and elongates the π-conjugation length, which results in a narrowing of the HOMO–LUMO energy gap. A systematic screening of the molecular structures using theoretical calculations reveals a further increase of the oscillator strength even without an ester group at the meso position, while a small difference for the excited state energies is expected (see Methods S1, Table S1, and Figure S1, Supporting Information). Therefore, TPATBC is expected to be a highly efficient NIR emitter that shows low E_{th}^{ASE} and E_{th}^{Laser} at longer wavelengths. Indeed, we have achieved one of the best E_{th}^{Laser} at above 800 nm from organic laser dyes owing to an unexpected shift of the spectrum.

Figure 1 shows the ultraviolet–visible (UV–vis) absorption and PL spectra of TPABC and TPATBC in toluene and 2 wt% doped films in poly(9,9-dioctylfluorene-*co*-benzothiaziazole) (F8BT) as a host prepared by spin-coating. F8BT was chosen owing to the low triplet excited state energy with the idea to effectively remove the emitter's triplet excitons under electrical excitation in our future study.[22] The characterization of the films in other conditions can be found in the Figure S2 and Table S2, Supporting Information. Although the TADF activity from TPATBC was also confirmed for the 6 wt% doped film of 4,4′-bis(carbazol-9-yl)biphenyl (CBP) with a higher triplet energy as a host, the Φ_{PL} was relatively low at 15%, suggesting a limited potential for use in OLEDs. The emission maxima of TPATBC were redshifted by ≈40 nm relative to those of TPABC in both solution and the blend films as was expected based on the theoretical calculations (**Table 1**). The calculated HOMO–LUMO energies were −5.42/−2.92 eV for TPABC and −5.29/−3.09 eV for TPATBC, respectively, which clearly revealed the narrower energy gap for TPATBC. In addition to the shift of the HOMO level, the LUMO level also became deeper with the introduction of thiophene, which was attributed to the increase of the conjugation length. Nevertheless, both compounds showed some overlap between the HOMO and LUMO (Figure S1, Supporting Information), which was assigned as a hybridized local-CT excited state.[23] The molar extinction coefficients (ε) at the absorption peaks were 1.7×10^5 and 1.1×10^5 L mol^{-1} cm^{-1} for TPABC and TPATBC, respectively. The decrease of ε in

Table 1. Optical properties of TPABC and TPATBC in toluene and 2 wt% F8BT blend films.

Compound	Condition	λ_{abs} [nm]	λ_{PL} [nm]	Φ_{PL} [b)] [–]	τ_f [ns]	k_r [10^8 s^{-1}]	k_{nr} [10^8 s^{-1}]
TPABC	In toluene	590	653	0.84	2.3	3.7	0.70
TPATBC	In toluene	612	690	0.57	1.9	3.0	2.3
TPABC	In blend film[a)]	600	685	0.82	2.2	3.7	0.82
TPATBC	In blend film[a)]	640	724	0.45	1.3	3.5	4.2

[a)]2 wt% doped in F8BT; [b)]Absolute PL quantum yield evaluated using an integrating sphere.

TPATBC, indicating a smaller overlap of the HOMO–LUMO wave functions, was also related to the CT properties that were more pronounced in TPATBC. In addition, the full width at half maximum (FWHM) of the absorption was 82 nm (2480 cm^{-1}) and 130 nm (3850 cm^{-1}) for TPABC and TPATBC, respectively. Moreover, the absorption and emission solvatochromisms were studied and TPATBC showed larger redshifts in polar solvents (Figure S3, Supporting Information). According to the Lippert–Mataga plot (Methods S2 and Figure S4, Supporting Information),[24–27] the change of the dipole moments between the S_0 and S_1 states ($\otimes\mu_{ge}$) was calculated to be $\otimes\mu_{ge}$ = 9 and 12 D for TPABC and TPATBC, respectively, suggesting a slightly higher intramolecular CT nature with the thiophene rings.

The blend films of TPABC and TPATBC in F8BT exhibited a Φ_{PL} of 82% and 45%, respectively, which were not so different from those in solution. The lower Φ_{PL} for TPATBC was attributed to the increase of nonradiative decay with a shifting of the spectrum to longer wavelength. However, k_r of TPABC and TPATBC were comparable as 3.7 × 10^8 and 3.5 × 10^8 s^{-1}, respectively (Table 1). These high values, especially at the emission maximum at >700 nm for TPATBC, were outstanding and proved the great potential to be a good laser material. The nonradiative rate constants (k_{nr}) of TPATBC were slightly larger than those of TPABC because of the smaller energy gap for TPATBC, while keeping it in small values compared to other NIR emitters, probably due to the negligible degree of bond length alternation and the relatively large HOMO–LUMO overlaps as mentioned above.[18] Here, we note that, as mentioned above, no TADF was found in the blend films owing to the low lying triplet excited state of F8BT.

The ASE properties of the spin-coated blend films were investigated using a nitrogen laser (excitation wavelength: 337 nm). **Figure 2** shows the ASE measurements of 2 wt% TPABC and TPATBC doped in a F8BT host layer at different excitation energies. Thin-film morphologies measured by atomic force microscopy (AFM) revealed smooth flat surfaces for these films (Figure S5, Supporting Information). Since the emitters showed strong aggregation-caused quenching, the lower doping concentrations showed a lower E_{th}^{ASE}, which were in accordance with the highest Φ_{PL} values. Note that the further decrease of the doping concentration such as 1 wt% caused insufficient energy transfer from the host. The results for different doping concentrations in the CBP and F8BT blend films are shown in the Table S3 and Figures S6 and S7, Supporting Information. At the high pumping intensities, a clear spectral line narrowing was observed, which was attributed to the amplification by stimulated emission in the organic waveguide layers. The E_{th}^{ASE} was determined by the intersection of the two slopes of the output intensity emitted from the edge of the films as a function of pumping intensity. The TPABC film showed an E_{th}^{ASE} as low as 9.9 μJ cm^{-2} at the ASE peak wavelength of 715 nm. On the other hand, ASE was observed at 807 nm for the TPATBC film. Although the E_{th}^{ASE} of 13.3 μJ cm^{-2} was slightly higher than that of TPABC, the ASE wavelength of TPATBC was significantly redshifted (>90 nm) from that of TPABC, which was considerably larger than that expected from their PL spectra.

In general, ASE occurs near the peak of the stimulated emission cross section (σ_{em}) spectra with a large optical gain, which can be calculated using the following equation: $\sigma_{em} = \lambda^4 E_f(\lambda)/(8\pi n^2[\lambda] c \tau_f)$, where λ is the wavelength, $E_f(\lambda)$ is the fluorescence quantum distribution, $n(\lambda)$ is the refractive index of the active gain layer, c is the speed of light, and τ_f is the fluorescence lifetime.[28,29] However, the existence of reabsorption from the ground and excited states is known to affect the optical amplification properties. Therefore, the effective σ_{em} (σ_{em-eff}) is defined by the following equation: $\sigma_{em-eff} = \sigma_{em} - (\sigma_{ABS} + \sigma_{SS} + \sigma_{TT})$, where σ_{ABS} is the absorption cross section of the ground-state species, σ_{SS} is the singlet–singlet excited-state absorption cross section, and σ_{TT} is the triplet–triplet excited-state absorption cross section.[30,31] The stimulated emission is inhibited when the σ_{em} spectrum largely overlaps with the absorption spectra. Since the excitation light source was short-pulse driven, the effect of σ_{TT} seemed to be negligible in this case. Here, the excited-state absorption spectra were measured using transient absorption spectroscopy (TAS) to verify the loss behavior for ASE. Note that solution samples in toluene were used for the TAS measurements, because clear signals could not be obtained for the film samples. However, the energy difference of S_0–S_1 in toluene and the F8BT film was <0.1 eV, which afforded sufficient data for the comparison of the overlap. Both of the TPABC and TPATBC compounds showed a clear singlet–singlet excited-state absorption band that decayed with a lifetime of 2.1 and 1.6 ns, respectively (Figure S8, Supporting Information). The spectra of σ_{em}, normalized ASE, ground state absorption, and singlet–singlet excited-state absorption are shown in **Figure 3**. The singlet–singlet absorption peaks for these compounds showed a relatively large difference in energy (≈0.35 eV), which should be discussed with the oscillator strengths for each excitation of S_1 to S_n in addition to the excited state levels, and the future successive study on detailed theoretical calculations is required to clarify the mechanism. For TPABC, the singlet–singlet absorption appeared at around 600 nm and there was almost no overlap with the emission spectrum. In addition, the ground state absorption seemed to cause only a small loss. Therefore, the ASE of TPABC clearly occurred close to the peak of σ_{em} (696 nm) based on the large optical gain window. In contrast, the ASE of TPATBC was apparently redshifted from the peak of σ_{em} (735 nm). Although the degree of the overlap between the emission spectra and ground state absorption spectra was similar for TPABC and TPATBC, the singlet–singlet absorption of TPATBC largely overlapped with the peak of the emission spectrum. Therefore, the net gain for the transition to the lower vibrational level of the ground state became small. However,

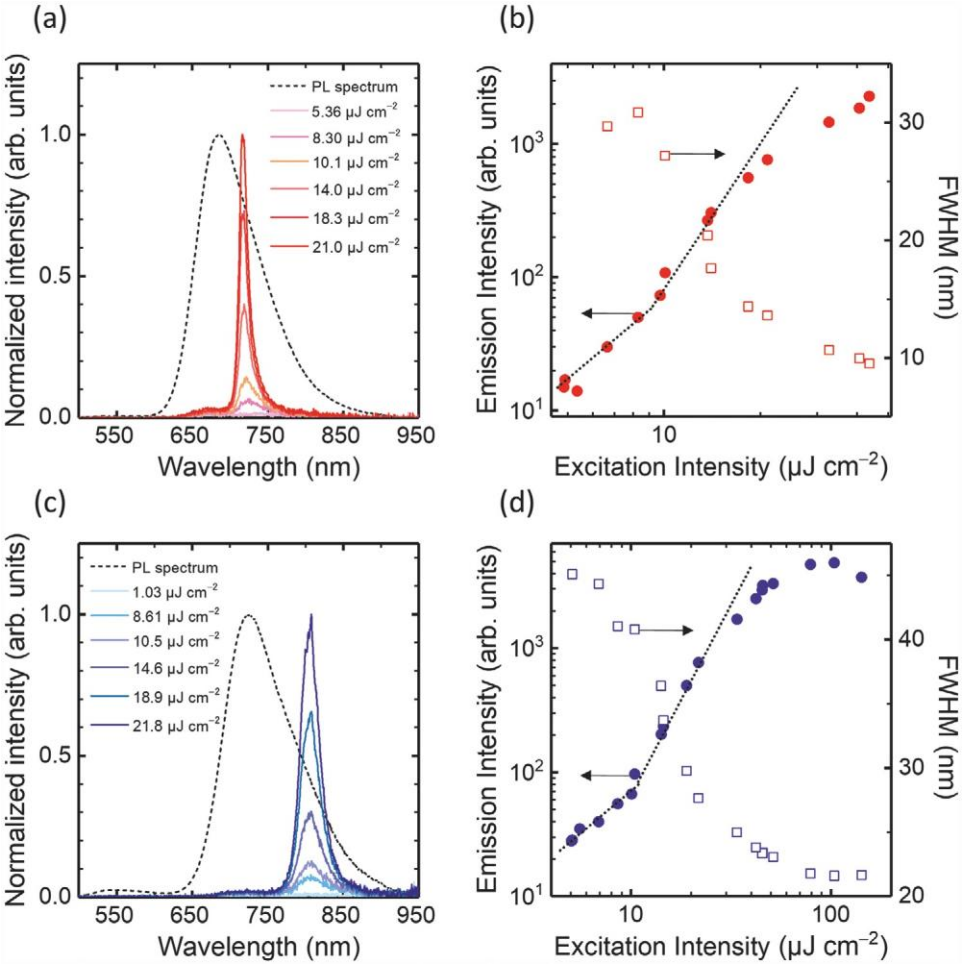

Figure 2. Steady-state PL and ASE spectra of a) TPABC and c) TPATBC measured at different excitation energies. Output intensity and full width at half maximum (FWHM) values as a function of excitation energy for b) TPABC and d) TPATBC (Reproducibility was confirmed by measuring three samples, for which $E_{th}^{ASE} = 14.1 \pm 0.8$ μJ cm^{-2}).

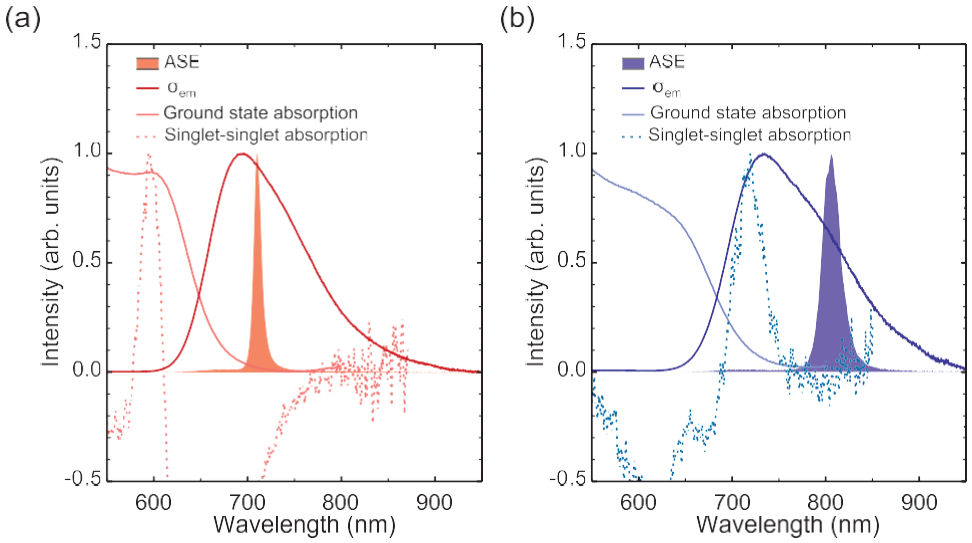

Figure 3. ASE, σ_{em}, and ground state absorption spectra in a 2 wt% F8BT blend film, and singlet excited-state absorption in toluene for a) TPABC and b) TPATBC. The peak intensity of the σ_{em} spectra was 3.1×10^{-16} and 2.1×10^{-16} cm^2 for TPABC and TPATBC, respectively. The peak intensity of the transient absorption spectra was 12.7 and 14.2 mOD for TPABC and TPATBC, respectively.

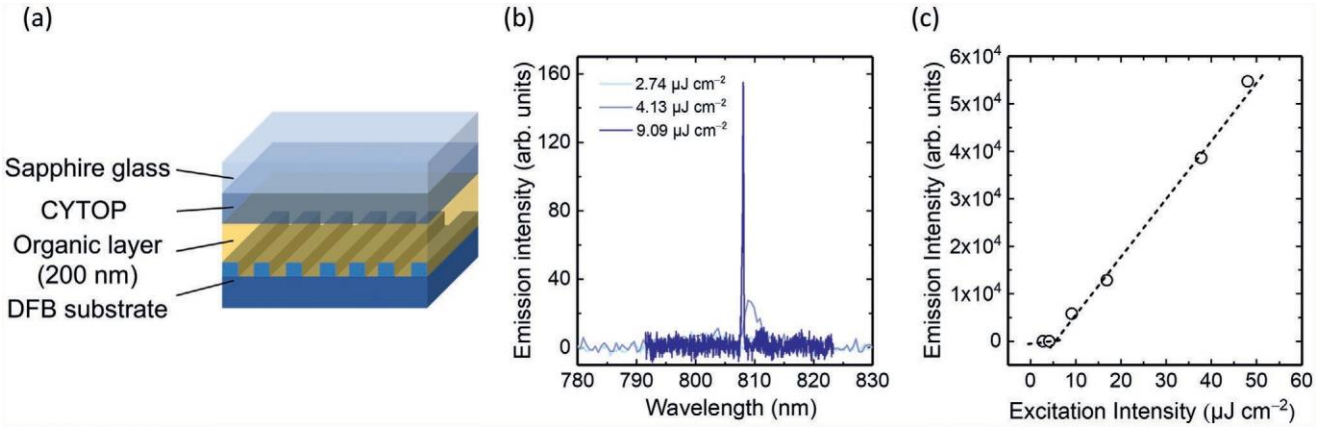

Figure 4. a) Schematic image of the DFB device. b) Emission spectra of TPATBC measured at different excitation energies. c) Output intensity as a function of excitation energy.

the transition to the higher vibrational levels was still capable of light amplification because of the intrinsically high σ_{em}. There have been some reports of a dual ASE behavior (referred to as 0–1 and 0–2 transitions) for compounds with reabsorption by the excited-state species,[32–35] which shows similarities with the case of TPATBC, but the loss in TPATBC was more strongly related to a specific region. Overall, the large redshift of the ASE can be ascribed to the shift of the vibrational levels in lasing. This behavior would be useful to shift the emission wavelength without largely sacrificing E_{th}^{ASE}.

Finally, the laser characteristics of the thin films of TPATBC were investigated using the second-order DFB resonators by optical pumping (see Experimental Section). The DFB grating architectures were designed according to the Bragg equation $m\lambda_{Bragg} = 2n_{eff}\Lambda_m$, where m is the order of diffraction, λ_{Bragg} is the Bragg wavelength, n_{eff} is the effective refractive index of the gain medium, and Λ is the period of the grating. The second-order ($m = 2$) grating provides an efficient vertical outcoupling of the laser radiation. Therefore, the grating periods (Λ_2) of 500, 510, and 520 nm, where the n_{eff} for the organic layers was 1.60, were chosen. Note that these grating periods are much larger than those for blue emitters, which is an advantage in terms of microfabrication processes. An organic layer was deposited on the DFB substrate and covered with a fluoropolymer (CYTOP) layer and a sapphire cover glass slide with a high thermal conductivity to minimize degradation (**Figure 4**). The lowest threshold was obtained for the DFB with a Λ_2 of 520 nm, where a sharp laser emission with a FWHM of 0.2 nm was observed at 807 nm above the E_{th}^{Laser} of 6.2 μJ cm^{-2}. This is one of the best values for laser thresholds with an emission above 800 nm.[36–39] Although the DFB with a smaller Λ_2 shifted the laser wavelength to higher energy, which agrees with the Bragg equation, the lasing thresholds were significantly increased (E_{th}^{Laser} of 86 μJ cm^{-2} at 780 nm for a Λ_2 of 500 nm and E_{th}^{Laser} of 8.9 μJ cm^{-2} at 793 nm for a Λ_2 of 510 nm, as shown in Figure S9, Supporting Information). This behavior also proved the presence of a large loss channel at <800 nm.

In this work, an advanced laser molecule, TPATBC, was developed and fully characterized. The emission maximum and the ASE peak were redshifted by ≈40 and 90 nm relative to those of TPABC, respectively. In addition, TPATBC showed a very low ASE threshold of 13.3 μJ cm^{-2} and a laser threshold of 6.2 μJ cm^{-2} in the NIR region. These results were attributed to the high k_r by the extension of π-conjugation and the precise control of donor–acceptor interactions. The further redshifts for ASE and laser wavelengths compared with the PL maxima arose from the lower energy transition at the next vibration level owing to the large overlap with the singlet–singlet excited-state absorption. As a result, an excellent NIR laser material with emission above 800 nm is found. We believe that our results are useful to design a laser emission at longer wavelengths, especially for NIR laser dyes.

Experimental Section

General: Commercially available materials were used as received from the suppliers. Details of instruments and physical measurements are given in Table S4, Supporting Information.

Synthesis and Characterizations: The synthetic procedures and characterization data for each material are described in Methods S3 and Figure S10, Supporting Information, and the NMR, HRMS and IR spectra are given in Data S1–S3, respectively, Supporting Information.

Film Sample Preparation: The thin films were prepared by spin-coating from chloroform solution (concentration: 15 mg mL^{-1}, 1800 rpm, 30 s at rt) onto precleaned fused silica substrates for optical measurements, onto non-fluorescent glass for ASE measurements, and onto 70-nm-SiO_2/glass substrate with a DFB pattern for laser measurements. The thicknesses of these films were measured using a Dektak profilometer and found to be typically around 200 nm.

Amplified Spontaneous Emission Measurement: The glass substrate with a thin film was cut at the center of the substrate along the scratch line. The measurements were performed in a nitrogen atmosphere to prevent degradation of the organic layer. N_2 gas lasers KEN2020 (Usho Optical Systems Co., Ltd., excitation wavelength at 337 nm, pulse width of 0.8 ns, frequency of 10 Hz) and NL100 (Stanford Research Systems, excitation wavelength at 337 nm, pulse width of 3.5 ns, frequency of 20 Hz) were used for the excitation. The laser light was focused into an area of 0.028 cm^2 using a slit and a cylindrical lens. The intensity of the excitation light was changed by using neutral density filters. The emission spectra from the edge of the sample depending on the excitation light intensity were measured using PMA12.

Distributed Feedback Laser Measurements: The second-order DFB grating was fabricated by electron beam lithography and reactive ion etching on the SiO_2. The laser characteristics of the thin film on the DFB lattice were investigated by optical pumping. Grating periods (Λ_2)

of 500, 510, and 520 nm were chosen based on the Bragg condition. The organic layer was covered with CYTOP (CTL-809M in CT-solv 180 from AGC) and a sapphire glass to prevent degradation. An N_2 gas laser NL100 was used for the excitation. The laser light was focused into an area of 0.00195 cm^2.

Transient Absorption Spectroscopy Measurements: The sample solutions were prepared in toluene at concentration of 1.0×10^{-5} M and used after deoxygenation with dry nitrogen gas. The YAG laser (355 nm) was used as a pump light, and the probe lamp was a xenon flash lamp.

Supporting Information

Supporting Information is available from the Wiley Online Library or from the author.

Acknowledgements

The authors thank Ms. K. Kusuhara and Ms. N. Nakamura for the characterization of materials, and Mr. M. Shiochi and Dr. S. Kobayashi for the measurements of AFM. This work was financially supported by JST ERATO Grant Number JPMJER1305 and the JSPS Core-to-Core Program. M.M. acknowledges JSPS KAKENHI Grant Number 19H02790, The Murata Science Foundation, and JSPS KAKENHI Grant Number 20K21227. J.W.W. acknowledges NRF grants (2017R1E1A1A01075394 and 2014M3A6B3063708).

Conflict of Interest

The authors declare no conflict of interest.

Keywords

amplified spontaneous emission, distributed feedback laser, organic light-emitting diodes, organic semiconductor laser diodes, thermally activated delayed fluorescence

Received: November 11, 2020
Revised: December 11, 2020
Published online:

[1] I. D. W. Samuel, G. A. Turnbull, *Chem. Rev.* **2007**, *107*, 1272.
[2] A. J. C. Kuehne, M. C. Gather, *Chem. Rev.* **2016**, *116*, 12823.
[3] S. Z. Bisri, T. Takenobu, Y. Iwasa, *J. Mater. Chem. C* **2014**, *2*, 2827.
[4] Y. Jiang, Y.-Y. Liu, X. Liu, H. Lin, K. Gao, W.-Y. Lai, W. Huang, *Chem. Soc. Rev.* **2020**, *49*, 5885.
[5] M. T. Hill, M. C. Gather, *Nat. Photonics* **2014**, *8*, 908.
[6] C. Adachi, A. S. D. Sandanayaka, *CCS Chem.* **2020**, *2*, 1203.
[7] C. Qin, A. S. D. Sandanayaka, C. Zhao, T. Matsushima, D. Zhang, T. Fujihara, C. Adachi, *Nature* **2020**, *585*, 53.
[8] X. Liu, M. Sang, J. Zhou, S. Xu, J. Zhang, Y. Yan, H. Lina, W.-Y. Lai, *Mater. Chem. Front.* **2020**, *4*, 3660.
[9] Y. Jiang, P. Lv, J.-Q. Pan, Y. Li, H. Lin, X.-W. Zhang, J. Wang, Y.-Y. Liu, Q. Wei, G.-C. Xing, W.-Y. Lai, W. Huang, *Adv. Funct. Mater.* **2019**, *29*, 1806719.
[10] S. K. Rajendran, M. Wei, H. Ohadi, A. Ruseckas, G. A. Turnbull, I. D. W. Samuel, *Adv. Opt. Mater.* **2019**, *7*, 1801791.
[11] M. Wei, M. Fang, S. K. Rajendran, W.-Y. Lai, G. A. Turnbull, I. D. W. Samuel, *Adv. Photonics Res.* **2021**, *2*, 2000044.
[12] A. S. D. Sandanayaka, T. Matsushima, F. Bencheikh, S. Terakawa, W. J. Potscavage, C. Qin, T. Fujihara, K. Goushi, J.-C. Ribierre, C. Adachi, *Appl. Phys. Express* **2019**, *12*, 061010.
[13] R. Weissleder, *Nat. Biotechnol.* **2001**, *19*, 316.
[14] C. Karnutsch, C. Pflumm, G. Heliotis, J. C. deMello, D. D. C. Bradley, J. Wang, T. Weimann, V. Haug, C. Gärtner, U. Lemmer, *Appl. Phys. Lett.* **2007**, *90*, 131104.
[15] J. V. Caspar, T. J. Meyer, *J. Phys. Chem.* **1983**, *87*, 952.
[16] Y.-C. Wei, S. F. Wang, Y. Hu, L.-S. Liao, D.-G. Chen, K.-H. Chang, C.-W. Wang, S.-H. Liu, W.-H. Chan, J.-L. Liao, W.-Y. Hung, T.-H. Wang, P.-T. Chen, H.-F. Hsu, Y. Chi, P.-T. Chou, *Nat. Photonics* **2020**, *14*, 570.
[17] M. Mamada, T. Fukunaga, F. Bencheikh, A. S. D. Sandanayaka, C. Adachi, *Adv. Funct. Mater.* **2018**, *28*, 1802130.
[18] D.-H. Kim, A. D'Aléo, X.-K. Chen, A. D. S. Sandanayaka, D. Yao, L. Zhao, T. Komino1, E. Zaborova, G. Canard, Y. Tsuchiya, E. Choi, J. W. Wu, F. Fages, J.-L. Brédas, J.-C. Ribierre, C. Adachi, *Nat. Photonics* **2018**, *12*, 98.
[19] J. Zhou, Z. Lu, X. Zhu, X. Wang, Y. Liao, Z. Ma, F. Li, *Biomaterials* **2013**, *34*, 9584.
[20] D. Jaque, F. Vetrone, *Nanoscale* **2012**, *4*, 4301.
[21] Y. Li, J. Ibanez-Guzman, *IEEE Signal Process. Mag.* **2020**, *37*, 50.
[22] S. Cook, H. Ohkita, J. R. Durrant, Y. Kim, J. J. Benson-Smith, J. Nelson, D. D. C. Bradley, *Appl. Phys. Lett.* **2006**, *89*, 101128.
[23] W. Li, Y. Pan, R. Xiao, Q. Peng, S. Zhang, D. Ma, F. Li, F. Shen, Y. Wang, B. Yang, Y. Ma, *Adv. Funct. Mater.* **2014**, *24*, 1609.
[24] E. Z. Lippert, *Electrochemistry* **1957**, *61*, 962.
[25] N. Mataga, Y. Kaifu, M. Koizumi, *Bull. Chem. Soc. Jpn.* **1956**, *29*, 465.
[26] R. M. Al-Moustafa, J. A. Degheili, D. Patra, B. R. Kaafarani, *J. Phys. Chem. A* **2009**, *113*, 1235.
[27] J. A. Degheili, R. M. Al-Moustafa, D. Patra, B. R. Kaafarani, *J. Phys. Chem. A* **2009**, *113*, 1244.
[28] A. V. Deshpande, A. Beidoun, A. Penzkofer, G. Wagenblast, *Chem. Phys.* **1990**, *142*, 123.
[29] X. Liu, C. Py, Y. Tao, Y. Li, J. Ding, M. Day, *Appl. Phys. Lett.* **2004**, *84*, 2727.
[30] A. S. D. Sandanayaka, T. Matsushima, F. Bencheikh, K. Yoshida, M. Inoue, T. Fujihara, K. Goushi, J.-C. Ribierre, C. Adachi, *Sci. Adv.* **2017**, *3*, e1602570.
[31] Y. Oyama, M. Mamada, A. Shukla, E. G. Moore, S.-C. Lo, E. B. Namdas, C. Adachi, *ACS Mater. Lett.* **2020**, *2*, 161.
[32] D. Fichou, S. Delysse, J.-M. Nunzi, *Adv. Mater.* **1997**, *9*, 1178.
[33] M. Polo, A. Camposeo, S. Tavazzi, L. Raimondo, P. Spearman, A. Papagni, R. Cingolani, D. Pisignano, *Appl. Phys. Lett.* **2008**, *92*, 083311.
[34] R. Kabe, H. Nakanotani, T. Sakanoue, M. Yahiro, C. Adachi, *Adv. Mater.* **2009**, *21*, 4034.
[35] M. Mamada, R. Komatsu, C. Adachi, *ACS Appl. Mater. Interfaces* **2020**, *12*, 28383.
[36] T. Kobayashi, J.-B. Savatier, G. Jordan, W. J. Blau, Y. Suzuki, T. Kaino, *Appl. Phys. Lett.* **2004**, *85*, 185.
[37] K. Yamashita, T. Kuro, K. Oe, H. Yanagi, *Appl. Phys. Lett.* **2006**, *88*, 241110.
[38] S. Yuyama, T. Nakajima, K. Yamashita, K. Oe, *Appl. Phys. Lett.* **2008**, *93*, 023306.
[39] H. Ye, D. H. Kim, X. Chen, A. S. D. Sandanayaka, J. U. Kim, E. Zaborova, G. Canard, Y. Tsuchiya, E. Y. Choi, J. W. Wu, F. Fages, J.-L. Bredas, A. D'Aléo, J.-C. Ribierre, C. Adachi, *Chem. Mater.* **2008**, *30*, 6702.